The Oviposition Inhibitory Neuron is a potential hub of multi-circuit integration in the Drosophila brain

Rhessa Weber Langstaff[1*], Pranjal Srivastava[3], Alexander B. Kunin[2], Gabrielle J. Gutierrez[1*]

***For correspondence:**
ggutierr@barnard.edu (GJG);
rweberla@barnard.edu (RWL)

[1]Department of Neuroscience and Behavior, Barnard College, New York, NY; [2]Department of Mathematics, Creighton University; [3]Department of Computer Science, Columbia University, New York, NY

Abstract Understanding how neural circuits integrate sensory and state information to support context-dependent behavior is a central issue in neuroscience. In Drosophila, oviposition is a complex process in which the fly integrates context and sensory information to choose an optimal location to lay her eggs. The circuit that controls the oviposition sequence is known, but how the circuit integrates multiple sensory modalities and internal states is not. We investigated the neural circuitry underlying high-level processing related to oviposition using the Hemibrain connectome. We identified the Oviposition Inhibitory Neuron (oviIN) as a key hub in the oviposition circuit and analyzed its inputs to uncover potential parallel pathways that may be responsible for computations related to high-level decision-making. We applied graph-theoretic analyses on the sub-connectome of inputs to the oviIN to identify modules of neurons that may constitute novel circuits. Our findings indicate that the inputs to oviIN form multiple parallel pathways from the unstructured neuropils of the Superior Protocerebrum where high-level computations have been known to occur.

Introduction

The fruit fly *Drosophila melanogaster* exhibits the capacity for complex behavior driven by neuronal circuits that carry out sophisticated brain computations (***Scheffer and Meinertzhagen, 2021***; ***Griffith, 2013***; ***Oram and Card, 2022***; ***Haberkern and Jayaraman, 2016***), with a nervous system consisting of over 100,000 neurons (***Dorkenwald et al., 2024***). Context-dependent computations, which conditionally process or integrate inputs, endow an animal with behavioral flexibility (***Hindmarsh Sten et al., 2021***; ***Roemschied et al., 2023***; ***Devineni et al., 2019***). For instance, hungry flies persistently track a food odor despite repeated failure to find food, showing that need is selectively reinforced in such conditions (***Sayin et al., 2019***). Context can even modulate egg-laying preference for acetic acid, despite the otherwise strong avoidance for the same food (***Joseph et al., 2009***). Processed sensory inputs integrate with context and state, in what we term high-level processing, to produce complex behavior.

Oviposition is a prime example of a behavior that relies on high-level processing (***Cury et al., 2019***; ***Yang et al., 2008***; ***Churchill et al., 2021***; ***Vijayan et al., 2023***; ***Cury and Axel, 2023***). Following mating, the female fly assesses a variety of factors such as the firmness (***Zhang et al., 2020***), taste (***Vijayan et al., 2022***; ***Joseph et al., 2009***; ***Yang et al., 2008***), and spatial attributes of a substrate (***Schwartz et al., 2012***), before deciding whether to deposit an egg. While sampling and evaluat-

ing multiple sensory inputs, the fly will compute a relative value for each encountered substrate (***Vijayan et al., 2023***; ***Yang et al., 2008***, ***2015***; ***Azanchi et al., 2013***). The fly will also consider social contexts and physical environment to optimize survival of the egg (***Rockwell and Grossfield, 1978***; ***Shelly, 1999***; ***Schwartz et al., 2012***). Computations such as these contribute to the complex decision-making process inherent in oviposition.

The circuit responsible for commanding the oviposition sequence and the cell types involved are known (***Wang et al., 2020***). After a mating experience, sex peptide inhibits the Sex Peptide Sensory Neurons (SPSN) and sex peptide abdominal ganglia (SAG) neurons (***Wang et al., 2020***; ***Feng et al., 2014***; ***Laturney et al., 2023***). The pC1a/b neurons downstream of SPSN and SAG are quieted by the reduced input which then also quiets the Oviposition Inhibitory Neuron (oviIN). The result is the disinhibition of the Oviposition Descending Neurons (oviDN) which elicit the oviposition motor action (***Wang et al.*** (***2020***); ***Figure 1***A). While this neural pathway is responsible for encoding and conveying mating status (***Yang et al., 2009***), it does not account for other computations that influence oviposition, such as the evaluations of substrate firmness and nutrient content, which depend on sensory inputs. The neural correlates of these computations are not yet well-defined; even so, we suppose that multiple circuits may converge onto the oviposition circuit to influence decision-making and eventually, egg-laying behavior. However, identifying these circuits within the vast network of the fruit fly brain presents a significant challenge (***O'Leary and Marder, 2014***). The recent advent of partial and full-brain connectomes provides a powerful resource for this investigation.

The currently available connectome datasets derive from electron microscope reconstructions of a female fruit fly's central brain (***Scheffer et al., 2020***; ***Dorkenwald et al., 2024***). The data comprehensively traces and annotates all the neurons in that volume including previously unknown neurons. It provides an extensive amount of morphological detail about individual neurons as well as cell type labels (***Schlegel et al., 2024***; ***Scheffer et al., 2020***). In particular, the connectome provides abundant detail about the locations and strengths of synapses among these neurons. The value of this publicly accessible dataset is that it provides the most comprehensive map of the connectivity in the fruit fly brain currently available.

We took the first step in identifying the key cell types that may be responsible for the high-level computations involved in oviposition. Our initial analyses reveal that the oviIN is a highly interconnected neuron in the oviposition circuit and in the brain. We employed a graph-theoretic approach to identify community structure among the inputs to the oviIN. This analysis revealed parallel pathways from diffuse regions of the central brain that impinge on the oviIN. These unstructured regions contain various critical circuits such as those related to oviposition (***Zhang et al., 2020***), circadian rhythms (***Li et al., 2018***; ***Shafer et al., 2022***), olfaction (***Wang et al., 2014***; ***Ruta et al., 2010***), and courtship (***Coleman et al., 2024***; ***Taisz et al., 2023***).

The Hemibrain data has primarily been used to study well-characterized regions of the brain such as the central complex (CX) (***Hulse et al., 2021***) and the Mushroom Body (MB) (***Li et al., 2020***). The cell types and connectivity profiles of the CX circuits that compute abstract internal representations of angular orientation, maintained by self-motion signals and visual cues, have been cataloged by ***Hulse et al.*** (***2021***). Furthermore, they found that the output types of the CX project to various parts of the brain, including premotor and sensory areas, and that they also return to the CX in a manner that evokes a deep recurrent network. The MB supports associative learning, enabling flies to pair odorants with positive and negative experiences (***Handler et al., 2019***; ***Aso et al., 2014a***,b). Investigations using the connectome and in vivo calcium imaging have led to a detailed understanding of how the anterior paired lateral neuron (APL) normalizes Kenyon cell signals (***Prisco et al., 2021***). The connectome has also aided researchers in discovering new MBON cell types that project outside of the MB lobes (***Li et al., 2020***) and that receive visual inputs as well as odor information (***Ganguly et al., 2024***; ***Li et al., 2020***).

While great advances have been made in understanding these well-studied areas of the brain, there remains significant potential to leverage this dataset to investigate less well understood re-

gions (***Scheffer and Meinertzhagen, 2021***; ***Lin et al., 2024***; ***Ito et al., 2014***). In our present study, we find that the inputs to oviIN predominantly come from the Superior Neuropils of the Protocerebrum (SNP) which have been known to support high-level processing for taste and water-seeking behavior (***Landayan et al., 2021***; ***Kim et al., 2017***), locomotion and olfactory responses (***Marquis and Wilson, 2022***), interactions between hunger and thirst (***Jourjine et al., 2016***), and persistent internal state of female flies (***Deutsch et al., 2020***), but we are far from a comprehensive map of functional circuits. Ultimately, determining the organization of oviIN's inputs will facilitate the discovery of novel circuits involved in high-level processing.

Results

oviIN is an outlier in the oviposition circuit and the brain

We queried the Hemibrain for the oviposition cell types from ***Wang et al.*** (***2020***) (***Figure 1***A) and found the quantity of presynaptic and postsynaptic connections (by synaptic weight; see Methods and Materials) made by each of the oviposition cell types (***Figure 1***B). The left instances are sometimes truncated and less complete than the right instances, thus left instances of oviposition cell types were excluded from the results. We were immediately struck by the oviIN because it makes far more synaptic connections than the other oviposition cell types (***Figure 1***B). Particularly relevant is the quantity of input connections to oviIN. The right oviIN has 21,624 synaptic input connections which is nearly 10 times as many inputs as the other oviposition neurons.

The oviIN makes abundant connections within the oviposition circuit (***Figure 1***C), particularly with SMP550 which is presumed to be the Oviposition Excitatory Neuron (oviEN; see ***Nojima et al.*** (***2021***)). As expected, oviIN is presynaptic to all subtypes of oviDN (including the putative additional pair of oviDNa that are labeled as SLP410 in the Hemibrain; see ***Nojima et al.*** (***2021***)) where it inhibits the initiation of the oviposition sequence. Among the pC1 neurons, oviIN receives inputs from all subtypes a-e and also sends outputs to subtypes b-e, forming a small recurrent motif. Notably, pC1c sends relatively weak outputs to oviIN but receives strong feedback from oviIN. While oviIN forms strong synaptic connections with many of the oviposition cell types, overall connections with the oviposition neurons make up a very small proportion of oviIN's synapses (<3%; ***Figure 1***D). It is clear from the Hemibrain data that oviIN makes a vast number of connections outside of the oviposition circuit.

Given that oviIN's extensive connectivity makes it an outlier in the oviposition circuit, we next sought to determine whether it is an outlier among the rest of the neurons in the Hemibrain with an eye towards other large inhibitory neurons. The Hemibrain provides information for all detected synaptic sites on the body of a traced neuron regardless of whether those synaptic sites are paired or functional. There are generally many more post sites than pre sites on a neuron's body due to the polyadic nature of synapses in the *D. melanogaster* brain. The counts of pre and post sites can be a useful quantification of the neuron's capacity to form synaptic connections. The Hemibrain also provides data for the synaptic connections between traced neurons. Those are reported as synaptic weights and are a count of the post sites that connect two neurons. As such, synaptic weight counts allow for comparisons of connection strengths that are not skewed by the polyadic imbalance between pre and post sites. However, since synaptic weight counts are only available for traced neurons, any connections made with untraced neurons are unaccounted for in the synaptic weight counts.

We found that the oviIN is one of the most synaptically endowed neurons in the Hemibrain. It is the 9th highest ranking neuron in the Hemibrain for total synaptic sites and the 6th highest ranking neuron for total synaptic connection weights (29,892 synaptic sites on oviIN_R; 50,898 synapse weights; ***Figure 2***a). The Anterior Paired Lateral (APL) neuron has the most synaptic sites on its body and the greatest amount of total synaptic connection weights (143,341 synaptic sites; 230,088 synapse weights) out of all the 21,739 traced, uncropped neurons in the Hemibrain dataset (***Figure 1***A). The APL has a role in normalizing the activity of odor-encoding Kenyon cells (***Prisco et al.,***

2021). In the synaptic site ranking, it is closely followed by the Dorsal Paired Medial (DPM) neurons (94,897 synaptic sites; 122,034 synapse weights), which are involved in odor memory and associative learning (***Waddell et al., 2000***; ***Keene et al., 2004***, ***2006***), and they are sleep-promoting (***Haynes et al., 2015***). The local Lateral Neurons (lLNs) of the antennal lobes also rank highly for synaptic sites and connection weights. Notably, these highly synaptically-endowed neurons are large inhibitory neurons (***Haynes et al., 2015***; ***Pitman et al., 2011***; ***Chou et al., 2010***). The average neuron in the Hemibrain has 1,148 synaptic sites and has a total of 1,565 synaptic connection weights. When considering the extent of oviIN's inputs separately, it ranks 13th for synaptic sites and connections weights (23,029 sites; 21,624 weights), making it an outlier in terms of the amount of input it receives.

The right oviIN ranks 7th for the number of total synaptic partners (pre and post) with 4,548 distinct partnering neurons, which is well above the mean number of partners for neurons in the Hemibrain (348.9), and which surpasses the other large inhibitory neurons. APL ranks 21st with 3464 partners, while the DPMs and lLNs have 3,030.5 and 3,553.5 on average, respectively. When considering only presynaptic partners, oviIN ranks 14th while APL ranks 2nd. The oviIN receives inputs from 2,524 neurons in the Hemibrain while the average neuron in the Hemibrain only receives inputs from 216 neurons.

The oviIN distinguishes itself from these other large inhibitory neurons with the number of cell types that it interacts with. With 1,379 cell types among its synaptic partners, oviIN ranks 15th in the Hemibrain on that metric (***Figure 2***B). Despite a high ranking for the total number of synaptic connections, APL only ranks 442nd in terms of the number of cell types among its direct connections with 493 types. The DPMs and lLNs connect with 192.0 and 296.5 types on average, respectively, while the average neuron in the Hemibrain makes direct connections with 139.2 cell types (***Figure 2***C). Notably, the oviIN ranks 5th when only taking into account the number of cell types that are presynaptic to it. The oviIN receives inputs from 968 cell types while the typical neuron in the Hemibrain receives inputs from 82 cell types.

Compared to the average neuron in the Hemibrain which makes connections in 4.8 primary neuropils, oviIN connects to about 3 times as many. The oviIN_R makes synaptic connections in 14 out of the 63 primary neuropils in the Hemibrain. Most of those connections are in the Superior Neuropils of the central brain.

"Hub-and-bespoke" structure among inputs to oviIN

Beyond the extraordinary quantity of synapses that oviIN makes, it is remarkable that oviIN is connected to so many distinct cell types that are broadly distributed across the brain. In light of oviIN's prodigious connectivity, we wondered whether it is a hub that integrates information from multiple circuits. It seems unlikely that all or most of the cell types that send inputs to oviIN are part of one large circuit that happens to span multiple brain areas, but the extent to which oviIN's inputs are composed of multiple parallel channels is unknown.

One could imagine that oviIN's extensive connectivity might be a result of it receiving small amounts of input from many different neurons. On the contrary, we find that oviIN's strongest presynaptic partners also favor oviIN as a postsynaptic partner. The oviIN is the prime target for the majority of cell types that strongly synapse on it. 60% of the cell types that send at least 120 synapse weights to oviIN also have oviIN as their strongest output. This is an indication of the primacy of oviIN to its presynaptic partners (***Figure 3***A). As might be expected, this primacy decreases for cell types that do not send strong connections to oviIN, indicating that those cell types prioritize making connections with other neurons besides oviIN. Taken together, the primacy of the strong inputs to oviIN indicates that these are cell types that exist to send input to oviIN.

The primary strong inputs to oviIN lay the foundations for potential circuit pathways to oviIN from other circuits, and their identities may be crucial for determining which circuits they funnel information from. However, the majority of cell types connecting to oviIN are uncharacterized, meaning they have either not been studied before being identified in the Hemibrain or they have not

yet been identified from existing scientific literature (***Figure 3***B). The Hemibrain provides generic labels to uncharacterized cell types that indicate the neuropil in which the bulk of their synapses are found, along with a 3-digit number (***Scheffer et al., 2020***). Neurons that have similar morphology and significant overlap in their synaptic connection patterns are assigned to the same cell type in the Hemibrain. A large proportion of inputs to oviIN have a cell type name that starts with SMP followed by a 3-digit number (27.9%), including the primary strong inputs to oviIN. SMP denotes the Superior Medial Protocerebrum, and all cell types that are labeled as SMP + 3-digit number are considered uncharacterized by the Hemibrain (see ***Scheffer et al.*** (***2020***) Appendix 1, Table 6). We note that ***Nojima et al.*** (***2021***) assert that the SMP550 is the oviEN but the Hemibrain has not updated its cell type label to reflect that proposition. Although the remaining SMP inputs to oviIN are uncharacterized, they might funnel information from known peripheral circuits to oviIN via the SMP.

The Superior Medial Protocerebrum (SMP) has historically been known as a "diffuse" neuropil (***Ito et al., 2014***). While the structured neuropils contain anatomical mappings of function, such as the wedges in Ellipsoid Body (EB) and the grid layout of Fan-shaped Body (FB), no such topological organization has been found for the diffuse neuropils of the Superior Protocerebrum (SNP) which includes the SMP, the Superior Intermediate Protocerebrum (SIP), and the Superior Lateral Protocerebrum (SLP). The SNP receives inputs from many other parts of the brain and may have a role in multi-circuit integration, higher-order processing, and context-dependent processing. For example, Dopaminergic neurons that project to the Superior Lateral Protocerebrum (SLP) influence the sucrose preferences of egg-laying flies (***Yang et al., 2015***; ***Marquis and Wilson, 2022***). The SNP has the potential to produce behaviorally-relevant computations on sensory inputs that influence oviposition, but the wiring logic of the SNP remains mysterious. Without a map of the SNP, we turned to a graph theoretic approach to determine the parallel structure of oviIN's inputs which may form independent or parallel pathways from peripheral circuits.

Modularity analysis reveals the parallel structure of oviIN's inputs

To begin to identify potential circuits connecting to oviIN, we sought to find the community structure of its inputs. We turned to the graph-theoretic framework of modularity for its ease of interpretation. Given a partition of nodes in a network, modularity measures the excess of within-group connections compared to a randomly-connected network (***Newman, 2006***). Maximizing modularity thus partitions the network into communities with higher within-group than between-group connectivity. Finding a partition which maximizes the modularity score can be done with machine-learning tools, such as RenEEL (***Guo et al.*** (***2019***); see Methods and Materials). By maximizing the Generalized Modularity Density score using the RenEEL algorithm, the optimal partitioning of an undirected network graph is found. Generalized Modularity is a multi-resolution method that can find community structure at various scales by adjusting the resolution parameter, χ. At a low resolution (χ = 0), the coarse structure of the network is returned as a small number of clusters with many neurons in each. As the resolution is increased (χ>0), the network is partitioned into a greater number of smaller clusters.

The partitions separate clusters of densely connected neurons into distinct communities, or modules, that may form the basis of a hierarchical circuit structure. Previous studies identified community structure in the whole Hemibrain connectome across multiple resolutions by maximizing Generalized Modularity Density (***Kunin et al., 2023***). This analysis recovered the gross structure of the brain by partitioning the neuropil super-structures. At higher resolutions, known fine structures, such as the sub-circuits of the layered FB, were recovered. In the current study, we limit our analysis to classical modularity (corresponding to the coarse resolution $\chi = 0$) on the input subconnectome of the right oviIN. The input subconnectome of oviIN contains all of its presynaptic partners and the connections among them. Only traced, non-cropped neurons were included in this sub-connectome in keeping with the analyses done by ***Kunin et al.*** (***2023***). This network was then converted into an undirected, weighted graph for input to the RenEEL algorithm. We applied

RenEEL to this sub-connectome to find mesoscale structure among the inputs to oviIN that is (1) specific to its inputs and (2) might otherwise be overshadowed by the community structure inherent to the full brain, even at higher resolutions. Our goal was to identify community structure that may otherwise be subsumed by the superstructure of the neuropils when analyzing the full Hemibrain. The modular structure we uncover depends on the relative connection strengths within and between groups; thus, by eliminating neurons that do not form direct connections to oviIN we can hope to identify densely-connected communities that potentially span multiple brain areas.

In the subnetwork of inputs to oviIN, RenEEL returned 7 modules containing from 199 to 347 neurons each. Each module contains between 111 and 199 unique cell types. The most prominent inputs to oviIN are spread among the different modules (***Figure 4***A), indicating that these modules may represent parallel pathways that each funnel distinct information to oviIN. The cell type that inputs most strongly to oviIN is the FS1A, a columnar output type of the Fan-shaped Body (FB). This cell type was first discovered in the Hemibrain and, as of now, no other experiments have been performed to characterize its effects on behavior. The FS1A mainly receives FB inputs from layers 2-6 and it leaves the FB to project outputs outside of the FB to the SMP and Crepine (***Hulse et al., 2021***). The FS1A is partitioned into the same module as the other FB types that send strong inputs to oviIN along with select, uncharacterized SMP cell types. The primary strong inputs to oviIN are also spread among the modules (***Figure 4***B), further supporting the notion that if oviIN is a hub, the primary strong inputs define the spokes that convey information from distinct circuits.

RenEEL was run 30+ times on the same sub-connectome data with different random seeds and it largely returned the same partitions. While this gives us confidence in the RenEEL algorithm's ability to detect fairly consistent communities within the subgraph consisting of the oviIN input connectome, it does not on its own confirm that RenEEL has uncovered mesoscale brain structure. To determine whether there is any spatial organization inherent in the modules, we visualized the input synapses to oviIN on its wire skeleton (***Figure 4***C). The input synapses on oviIN are shown as dots and each dot is colored according to the module of the presynaptic neuron. Neurons from modules 1, 3 and 7 mostly synapse onto oviIN within the dorsal tuft of processes within the SMP where most of oviIN's output sites also reside. Neurons from modules 4 and 6 also form most of their synapses onto oviIN within the dorsal tuft, but they also have a large portion of synapses in the inferior neuropils along the posterior and anterior part of the Crepine, respectively. Module 5 neurons predominantly form their synapses to oviIN along the anterior Crepine, but also occupy portions of the dorsal tuft. Neurons from module 2 mainly form their connections along the ventral portion of the oviIN intersecting with lateral complex, ventromedial and inferior neuropils. The anatomical organization of modules indicates that RenEEL found biophysically meaningful groupings of neurons. The modules do not simply reflect the boundaries of the neuropils that intersect with oviIN because all of the module synapses intersect with a mixture of neuropils and they all intersect to some extent with the SNP (***figure Supplement 1***). The organization along the distinct branches of oviIN suggests that neurons work together with the other neurons in their module to influence the activity within different regions of this large neuron. It is possible that the motifs within these modules act as local processing units to drive, summate, or shunt activity from other local processing units.

It is reasonable to wonder whether the anatomical organization of the modules is a reflection of the neuropil organization of the brain more broadly, rather than the neuropil boundaries of the synapses on oviIN. In other words, has RenEEL clustered oviIN's inputs according to the neuropils that they "belong to"? Strictly speaking, neurons cannot easily be classified as belonging exclusively to one neuropil because they often make connections in multiple neuropils, although researchers sometimes classify a neuron based on the neuropil where it makes the majority of its synaptic contacts (***Scheffer et al., 2020***; ***Schlegel et al., 2024***; ***Ito et al., 2014***). To determine the various brain regions that are represented among the inputs to oviIN, we queried the Hemibrain for the neuropils in which oviIN's presynaptic partners make synaptic connections with any neuron, including but not limited to oviIN (***Figure 5***A, pie charts). RenEEL did not partition oviIN's input connectome

according to the neuropils where those neurons form their connections. In all but modules 2 and 5, the neurons form the majority of their synapses in the SNP. We had already determined that, collectively, the majority of oviIN's inputs are made in the SNP (***Figure 3***B), and that a large proportion of oviIN's input connectome contains neurons that are labeled as SNP neurons. ***Figure 5***A shows that RenEEL has identified SNP sub-groups that may pertain to distinct SNP circuits. We note that neuropil designations are primarily driven by anatomical considerations and do not necessarily demarcate functional circuits. Thus, the modules may represent circuit structure that draws from SNP together with other neuropils. For example, the most prominent cell type input to oviIN, FS1A, is in module 4. The FS1A neurons receive most of their input connections in the FB neuropil of the CX, but they make most of their output connections in the SMP (of the SNP) and CRE (of the INP) (***Hulse et al., 2021***). Such uncharacterized cell types may form a bridge from one part of the brain to the SNP, INP, LX, or VMNP neuropils where they interact with oviIN.

We next wondered whether the partitions found for oviIN's input connectome reflect those previously found for the full Hemibrain connectome. The coarse modules found in the full Hemibrain connectome were roughly aligned with the neuropil structure of the brain, indicating that RenEEL identified macroscale brain structure that is aligned with the functional aspects of the neuropils. As we only consider neurons which make direct synaptic contact with oviIN_R in the present study, we do not expect exact agreement between our identified modules and those that would be identified in the full Hemibrain network, nor a full connectome of the Drosophila brain, but we might expect strong alignment if that super-structure is present within the sub-connectome of oviIN's inputs. We compared our results to the modules identified by ***Kunin et al.*** (***2023***), and we found that the portion of oviIN's input connectome that resides in full Hemibrain module 3 (which corresponds mostly to SMP and SIP) is spread out among all of the sub-connectome modules (***Figure 5***B). In other words, large portions of the neurons in the sub-connectome modules all share a common module in the full Hemibrain clustering - namely the module that encompasses the medial and intermediate superior neuropils. Full Hemibrain module 1 corresponds mainly to VMNP, and the portion of oviIN's connectome that is from that area is dominated by sub-connectome module 2. Likewise, full Hemibrain module 2 which corresponds to FB is mainly represented in sub-connectome module 4. However, all of the sub-connectome modules are composed of a combination of full Hemibrain modules. In particular, every cluster identified in oviIN's connectome has significant overlap with the full Hemibrain cluster that largely encompasses the superior intermediate and superior medial neuropils (SIP, SMP). This suggests that, in the full Hemibrain, the connections within SNP are stronger overall than connections between SNP and other neuropils, and that mesoscale connections within potential circuits that include SNP neurons combined with other cell types are dense enough to be detected in the absence of the connections with the broader network of each neuropil.

To determine whether the coarse modules of oviIN's input connectome correspond to mid-resolution modules of the full Hemibrain, we computed the Jaccard similarity between each coarse cluster in the sub-connectome of oviIN's inputs and the clusterings of the full Hemibrain at various resolutions (***Figure 5***C). A high Jaccard similarity is an indication that many pairs of neurons are partitioned into a module together in both the sub-connectome clustering and the full Hemibrain clustering at a particular resolution. With fewer modules for the lower resolutions, it is more likely for pairs of neurons to be within the same modules; however, the mean similarity of the sub-connectome clusters in comparison to the coarse Hemibrain clusters is only about 0.7 which indicates that there is not perfect overlap between those two clusterings. Furthermore, there are no higher resolutions of the Hemibrain clustering at which average similarity increases beyond that for the coarse Hemibrain clustering. Thus, applying RenEEL to a sub-connectome of the brain, as we have done for oviIN's input connectome, does not partition the neurons into the same cluster as for the full connectome, either at the same or at a higher resolution. Our results suggest that the modules correspond to a microscale organization at the level of oviIN's parallel inputs – which may correspond to distinct circuit pathways and which may have functional significance for oviIN.

To verify that these modules are representatives of distinct parallel circuits feeding into oviIN, we considered their connections within the full Hemibrain. We computed the similarity of inputs from anywhere in the brain to each pair of neurons in oviIN's input connectome (see Methods and Materials). On average, the similarity of within-module pairs exceeds those of between-module pairs (***Figure 6***A). In other words, presynaptic partners of oviIN have more of their inputs in common with other neurons in their same module than with neurons in a different module. Moreover, comparison to a randomly partitioned network reveals that within-module pairs are significantly more similar than would be seen by chance (***Figure 6***B). This supports the idea that the modules represent parallel streams of input from different circuits.

Discussion

The complexity inherent in the decision-making and behavior of *Drosophila* makes studying its tiny brain a worthwhile endeavor because isolating the circuits that drive high-level processing is within reach. The Drosophila brain has a hierarchical organization where peripheral sensory inputs undergo multiple stages of higher order processing, evident in both the adult (***Jeanne et al., 2018***; ***Kunin et al., 2023***) and larval brain (***Winding et al., 2023***; ***Betzel et al., 2024***). Researchers have made progress studying the sensory periphery and progressively discovering higher-order neurons and circuits (***Walker et al., 2024***; ***Jacobs et al., 2024***; ***Matsliah et al., 2024***), but such an approach is inadequate for discovering the circuits that drive the complex computations involved in context-dependent decision-making. Behaviors like oviposition depend on nearly every sensory modality, and starting at the periphery to discover the high-level circuits that integrate sensory inputs, state, and memory would require an expansive search. The connectome now offers another way to discover the neural circuits that are responsible for high-level processing. In the approach put forth in the present study, we begin by targeting the known terminal circuit in the connectome that is responsible for commanding oviposition (***Wang et al., 2020***). We worked backwards from the command circuit and we analyzed its inputs to study the neural correlates for the highest level computations that drive oviposition. Given that the inputs are largely uncharacterized cell types, our goal was to identify the structural pathways into the oviposition circuit so that future work could determine the sensory and functional bases for these input pathways.

To summarize our findings, we first observed that the oviIN is an outlier in the oviposition circuit and in the brain due to its abundant connectivity within and beyond the oviposition circuit. The vast majority of inputs to oviIN are uncharacterized cell types, but our analyses revealed potential parallel circuit pathways to oviIN. First, a large proportion of the strongest inputs to oviIN have oviIN as their strongest output, suggesting that oviIN is a primary target of multiple neurons rather than simply collecting small amounts of input from many neurons that primarily send outputs elsewhere. Second, modularity analysis showed that the primary strong inputs to oviIN are distributed across multiple modules indicating multiple parallel pathways among the primary strong inputs. Furthermore, we show that our modularity results do not reflect the same scope of anatomical organization that was found for the full Hemibrain modules by ***Kunin et al.*** (***2023***). Instead, performing modularity on the subconnectome containing oviIN's inputs reveals an anatomical organization at a biophysically relevant scale for oviIN. Finally, we show that there is higher similarity among the inputs to neurons within a module than across modules, which further supports the parallel structure of the input modules. Together, these findings suggest that the inputs to oviIN represent multiple parallel pathways from high-level processing circuits.

High-level processing in SNP

The majority of oviIN's inputs come from the SNP – a mysterious region that includes the SLP, SIP, and SMP neuropils and that lacks a topological organization (***Ito et al., 2014***). The literature shows that this area is rife with high-level processing potential. MBONs carry odor information and they send projections to the SNP at convergence zones where their synapses are modulated by experience (***Aso et al., 2014a***). Sensory and interoceptive inputs to the subesophageal zone are

relayed to the Superior Medial Protocerebrum (SMP) where they regulate water and food seeking behavior (***Jourjine et al., 2016***; ***Landayan et al., 2021***). Taste projection neurons that project to the SLP are essential for conditioned taste aversion whereas those that bypass the SLP are not (***Kim et al., 2017***). With regards to oviposition, Dopaminergic neurons that project to the SLP influence the sucrose preferences of egg-laying flies (***Yang et al., 2015***). The sexually dimorphic pC1 neurons have a role in persistent states related to courtship and aggression (***Deutsch et al., 2020***; ***Zhou et al., 2014***). They are presynaptic to oviIN, and according to the Hemibrain, they make most of their synapses in the SNP as well. Despite these behaviorally relevant functions, the SNP remains *"terra incognita"* as far as its organization (***Scheffer et al., 2020***).

Without a pre-existing map of the SNP or a comprehensive wiring logic for it, our results point to clusters of mainly uncharacterized cell types that may form high-level circuits that do computations that are relevant for oviposition. To be clear, we do not claim to have identified complete circuits since our approach intentionally limited our analysis to the connectivity among the neurons that directly input to oviIN. Rather, our coarse clustering casts a wide net around the primary strong inputs to oviIN to dredge up clues about the regions and circuits that are associated with its inputs. Future experimental and computational work will be needed to fully characterize the potential circuits that our analysis has indicated.

Selective application of modularity for structural scope

Discovering communities within connectome graphs often relies on spectral methods to form clusters of nodes by creating a graph embedding (***Chung et al., 2021***). Alternatively, we chose to detect communities within the sub-connectome of oviIN's inputs using the RenEEL algorithm to perform modularity analysis. Modularity offers ease of interpretability: the resulting clusters, or modules, consist of the nodes that are more highly interconnected among themselves than they are to other modules (***Newman, 2006***; ***Newman and Girvan, 2004***; ***Guo et al., 2023***; ***Kunin et al., 2023***).

In our study, we chose to apply modularity to a subnetwork of the connectome to control the scope of the structure we were probing. Modularity was previously applied to the full Hemibrain connectome by ***Kunin et al.*** (***2023***) and had recovered gross anatomical structure that reflects the neuropil organization of the brain, as well as finer structure such as the layers of the FB. While such anatomical structure often underlies functional circuit structure, it might obscure mesoscale and microscale circuit structure that is not necessarily contained within a given neuropil. For example, the FS1A and the SMP133 neurons are from different neuropils and they are clustered into separate modules for the full Hemibrain connectome. However, they are clustered into the same module when the modularity analysis is applied to the sub-connectome of oviIN's inputs. These neurons are separately partitioned in the full connectome because the connections they make with other neurons from their own neuropil are denser than any connections made with neurons outside of their neuropils. However, when the scope of the network is limited only to neurons that are (at least putatively) involved in a particular function, such as oviposition, the interactions between these neurons becomes more apparent. That FS1A and SMP133 are associated within the same module suggests a functional relationship. By applying modularity to a subnetwork consisting of the inputs to oviIN, we limited our analysis to finding partitions at a microscale level of relevance.

Generalized modularity offers another way in which to probe mesoscale and microscale structure. The resolution parameter, χ, can be adjusted to retrieve more modules containing fewer neurons. With the full Hemibrain network, the hierarchically nested anatomical structure was revealed at higher resolutions – the modules identified at higher resolutions were generally subsets of the coarsest modules, though this partition was not always strict (***Kunin et al., 2023***). Even still, the fine modules of the full Hemibrain did not correspond to the coarse modules that we obtained for the subconnectome consisting of the inputs to oviIN (***Figure 5***). This demonstrates that classical modularity on a subconnectome does not produce the same results as generalized modularity at higher resolutions on a full connectome. Although our study did not set out to investigate the subtleties between classical and generalized modularity analysis, we propose that applying classical

modularity to a sub-connectome targets a different scope of brain structure than applying generalized modularity on the full connectome. While the resolution parameter can be used to probe nested anatomical structure in the full Hemibrain, we propose that biophyically-relevant, circuit-specific microscale structure can be targeted by constraining the network to a sub-connectome as we have done.

Our study did not utilize higher modularity resolutions to characterize the subconnectome of oviIN's inputs. We found that at a high resolution ($\chi = 1.0$), modularity tended to form clusters of cell types (results not shown) as was also true for higher resolutions of the full Hemibrain (***Kunin et al., 2023***). However, we might expect the intermediate resolutions to further subdivide modules to find maximally distinct input pathways to oviIN since currently it is possible that a single coarse module contains one or more input pathways. Future work will attempt to refine the use of generalized modularity on a subconnectome by incorporating centrality metrics and participation scores.

Future Directions

Our study is limited to a connectome consisting of classical chemical synapses. Although electrical synapses and neuropeptides play an important role in the computations and functions of the fly brain, gap junctions and neuropeptide release sites are not included in the current connectome data. Future iterations of Drosophila connectomes may include these additional features, enabling us to build upon the results we present here.

In conclusion, we have presented evidence that the oviIN integrates multiple distinct pathways of inputs. These inputs presumably contribute to the complex processing done by the ovipositing female fly and may lead us to novel high-level circuits in the uncharted regions of the SNP. Future work will continue to probe these input pathways to characterize their wiring logic. Concurrently, new methods for identifying novel circuits from connectome data will have to be developed since this is a new area and a new dataset. It is our hope this will lead to identifying key cell types within those circuits so that experimentally testable hypotheses can be presented.

Methods and Materials

Accessing and working with the Hemibrain connectome data

All analyses presented were performed using the publicly available Hemibrain connectome data released by Janelia (***Scheffer et al., 2020***). The data are from an EM reconstruction of the right hemisphere and partial left hemisphere of a single female fly brain. Morphological data for the 3D reconstruction was accessed, along with tabular data of the neuron annotations and connectivity, using the Neuprint python package released by Janelia (https://github.com/connectome-neuprint/neuprint-python). The data accessed via Neuprint is Hemibrain version 1.2.1. For the brain-wide rankings (***Figure 2***), we relied on the most recent table of traced neurons made available by Janelia (https://storage.cloud.google.com/hemibrain/v1.2/exported-traced-adjacencies-v1.2.tar.gz) which is version 1.2, and which contains only neurons that are traced and not cropped.

Every contiguous object in the Hemibrain is assigned a unique bodyId, and many of these are also assigned a cell type. Janelia annotated cell types based on their morphology and shared connectivity patterns. There are some traced, uncropped neurons that are not assigned a cell type. These are labeled as "None" and were excluded from certain analyses wherever indicated. Janelia also annotates neurons with an instance label that can be used to differentiate between right and left instances of bilateral cell types. For example, there are 2 neurons in the Hemibrain of the oviIN cell type: a right and a left instance that are denoted as oviIN_R and oviIN_L, respectively. Our analyses largely focused on the right oviIN.

Neurons in the Hemibrain that match with neurons that have been empirically characterized in the literature are typically annotated with their known name, thus we denote these as known cell types. Neurons that have not been characterized are often given a cell type name that begins

with the abbreviation for the neuropil where most of its synaptic contacts are located followed by a 3-digit number where the numbering sequence begins with 001. Neurons such as these may have been previously characterized in the literature but have not been matched in the Hemibrain. One example is SMP550 which is presumed by ***Nojima et al.*** (***2021***) to be the oviEN identified by ***Wang et al.*** (***2020***). Except for this particular case, we denote uncharacterized cell types as unknown along with unnamed cell types ('None').

Drosophila synapses are polyadic, meaning that multiple postsynaptic densities can be associated with a single presynaptic T-bar. The Hemibrain provides counts of the postsynaptic density sites as well as counts of the presynaptic sites on the bodies of anything that is given a bodyId, as well as locations in 3D space of those sites. Additionally, the Hemibrain provides data for the synaptic connections among neurons in the 3D reconstruction. These are given as synaptic weights where the weight is the count of postsynaptic sites within the synapses that connect two neurons.

Primacy of outputs to oviIN

A neuron or cell type is considered a prime input to oviIN if it has oviIN as its strongest output. This is determined on a by-neuron basis by querying the synaptic outputs of a neuron and ordering by descending weight. It is determined on a by-cell type basis by querying the synaptic outputs of all the neurons of a given cell type, summing those weights by postsynaptic cell type, and putting those aggregated weights in descending order (***Figure 4***B). The position of the oviIN type in the list determines the primacy of oviIN as an output. If oviIN is in the 0th position of outputs from a neuron, that neuron is a prime input to oviIN.

Parsing neuropil data

When fetching adjacencies between neurons or cell types in the Hemibrain, the data indicates the neuropil, or region of interest (ROI), in which the connection is located. For consistency and clarity, we merged right and left ROIs and relabel primary ROIs with their corresponding supercategory of neuropil according to ***Ito et al.*** (***2014***).

For pie chart visualizations in which the data were restricted to synapses made with oviIN (***figure Supplement 1***), the synapse weights between oviIN_R and its presynaptic partners were queried by ROI. For each module, the synapse weights from module neurons onto oviIN were summed within each ROI, thus providing the total synapse weights onto oviIN_R made within each ROI by the neurons in a given module. For the pie chart visualization in ***Figure 5***A all synapse weights involving presynaptic partners of oviIN were queried – including synapses made with neurons other than oviIN. For each neuron, the proportion of synapses made within each ROI were calculated by totaling the synapse weights made by the neuron in that ROI and dividing by the total synapse weights made by the neuron in all the ROIs. These proportions were tallied up by ROI within each module. The pie slices represent the proportion of connections made within each ROI by all the neurons in a module, but normalized on a per neuron basis.

RenEEL algorithm for computing generalized modularity

The set of neurons presynaptic to oviIN and the synaptic connections among them were converted into an undirected, weighted graph. The weight of each edge was computed as the total synaptic weights between the two neurons. The community structure of this network was identified with the partition $\mathcal{C} = \{C_1, C_2, \dots\}$ maximizing the generalized modularity density score (***Guo et al., 2023***),

$$Q_g = \sum_{C \in \mathcal{C}} \left(\frac{m_C}{m} - \left(\frac{K_C}{2m} \right)^2 \right) \rho_C^{\chi}$$

The sum is taken over communities C; m is the total number of edges in the network, m_C is the total weight of edges in community C, K_C is the weight-degree sum of nodes in C (the sum of the weights of edges incident to each node in C), and ρ_C is the relative density of connections in C,

defined by

$$\rho_C = \frac{2m_C}{n_C(n_C - 1)}$$

Where n_C is the number of nodes in community C. The exponent χ controls the resolution of the clustering. We consider $\chi \geq 0$. At $\chi = 0$, Q_g equals the classic Modularity (***Newman, 2006***), with $\chi > 0$ resolving smaller, more densely-connected communities (***Guo et al., 2019***, ***2023***).

We used RenEEL, a machine-learning based approach for network clustering, to identify the partition $\mathcal{C}$ which maximizes the generalized modularity density (***Guo et al., 2023***). RenEEL first creates an ensemble of candidate partitions using a fast heuristic. The ensemble is iteratively updated, alternating steps of reducing and replacing. In the reducing step, each community identified by all partitions in the ensemble is combined to a single node. In the replacing step, the fast heuristic is used again on the reduced network. If the result matches one of the previous partitions, or has a lower score than any of the ensemble partitions, the ensemble size is reduced by one. Otherwise, the result replaces the ensemble partition with the lowest modularity score. This process repeats until only one partition remains in the ensemble, representing a consensus best partition. We used an implementation that has previously been shown to produce fast and accurate results for networks of the size and density we consider (***Guo et al., 2019***, ***2023***; ***Kunin et al., 2023***). The source code is available on Github: https://github.com/prameshsingh/generalized-modularity-density.

In our study, RenEEL was applied to the sub-connectome of oviIN_R inputs which consists of all the presynaptic partners to oviIN_R and the connections among them. The results presented are from a representative run that resulted in a single set of partitions, $\mathcal{C}$. RenEEL was subsequently run on the same sub-connectome 50 times with different random seeds to determine that partitions were largely consistent between runs. When analyzing and making comparisons to the modularity of the full Hemibrain, RenEEL results from ***Kunin et al.*** (***2023***) were used.

Analyses and Visualizations

All analyses and visualizations were done in Python using custom-written scripts along with various published and open-source packages (see Methods sections for relevant packages). Our analysis code is publicly available on GitHub: https://github.com/orgs/Gutierrez-lab/oviIN-inputs.

Joint clustering plots

We compared the the modularity results for the oviIN_R inputs sub-connectome and the full Hemibrain connectome. We computed the proportion of nodes from a module in one clustering that are partitioned into a module from another clustering. The joint counts between the coarse resolutions (χ=0.0) in both modularity datasets were computed. The width and height of the boxes represent the joint counts of neurons within two modules over the total counts within a module of the respective dataset (***Figure 5***B).

Jaccard Similarity

To evaluate the similarity between different neuron clusterings $\mathcal{A}$ and $\mathcal{B}$, we compute the Jaccard similarity. For a set of neurons $\{1, 2, 3, \ldots N\}$, Jaccard Similarity considers all pairs of neurons in the set and is defined as:

$$J(\mathcal{A}, \mathcal{B}) = \frac{\sum_{i=1}^{N} \sum_{j=i+1}^{N} \mathbf{1}\{C_i^{\mathcal{A}} = C_j^{\mathcal{A}} \textit{ and } C_i^{\mathcal{B}} = C_j^{\mathcal{B}}\}}{\sum_{i=1}^{N} \sum_{j=i+1}^{N} \mathbf{1}\{C_i^{\mathcal{A}} = C_j^{\mathcal{A}} \textit{ or } C_i^{\mathcal{B}} = C_j^{\mathcal{B}}\}}$$

where N is the total number of neurons in the set, $C_i^{\mathcal{A}}$ and $C_i^{\mathcal{B}}$ are the cluster assignments of neuron i in clusterings $\mathcal{A}$ and $\mathcal{B}$, respectively. The indicator function $\mathbf{1}\{\cdot\}$ equals 1 if the condition inside is true and 0 otherwise.

The Jaccard similarity ranges from 0 to 1. A value of 0 indicates no overlap between the clusterings, while a value of 1 indicates complete overlap for neurons that are in the same cluster in the set.

In our study, we applied this method to compare the clustering of the oviIn inputs with the clustering of the entire Hemibrain for different resolutions of RenEEL algorithm. The similarity analysis was performed for the set of neurons in each cluster in the sub-connectome separately.

Input Similarity

Input similarity was computed as the cosine distance between the vectors representing the inputs to each neuron. For every neuron n, we compute the vector n_{in} of length equal to the number of neurons in the Hemibrain, with the ith entry equal to the synapse weight from neuron i to neuron n. If neuron i is not synaptically connected to neuron n, the corresponding entry is 0. For two vectors u, v the cosine distance is given by $d_{cos}(u, v) = \langle u, v \rangle / \|u\| \|v\|$. Because all entries in n_{in} are nonnegative, cosine similarity ranges between 0 and 1. A similarity of 0 means that two neurons receive inputs from completely disjoint sets of neurons; a similarity of 1 means they receive inputs from exactly the same neurons in exactly the same proportion.

Mean similarity was computed within modules by averaging over all pairs of distinct neurons belonging to that module, and across modules by averaging over all pairs with one neuron in each cluster. For comparison, we shuffled module membership, preserving the size of each module but randomly assigning module numbers to each neuron. The mean similarity within each module was well outside the distribution obtained from 100 shuffles.

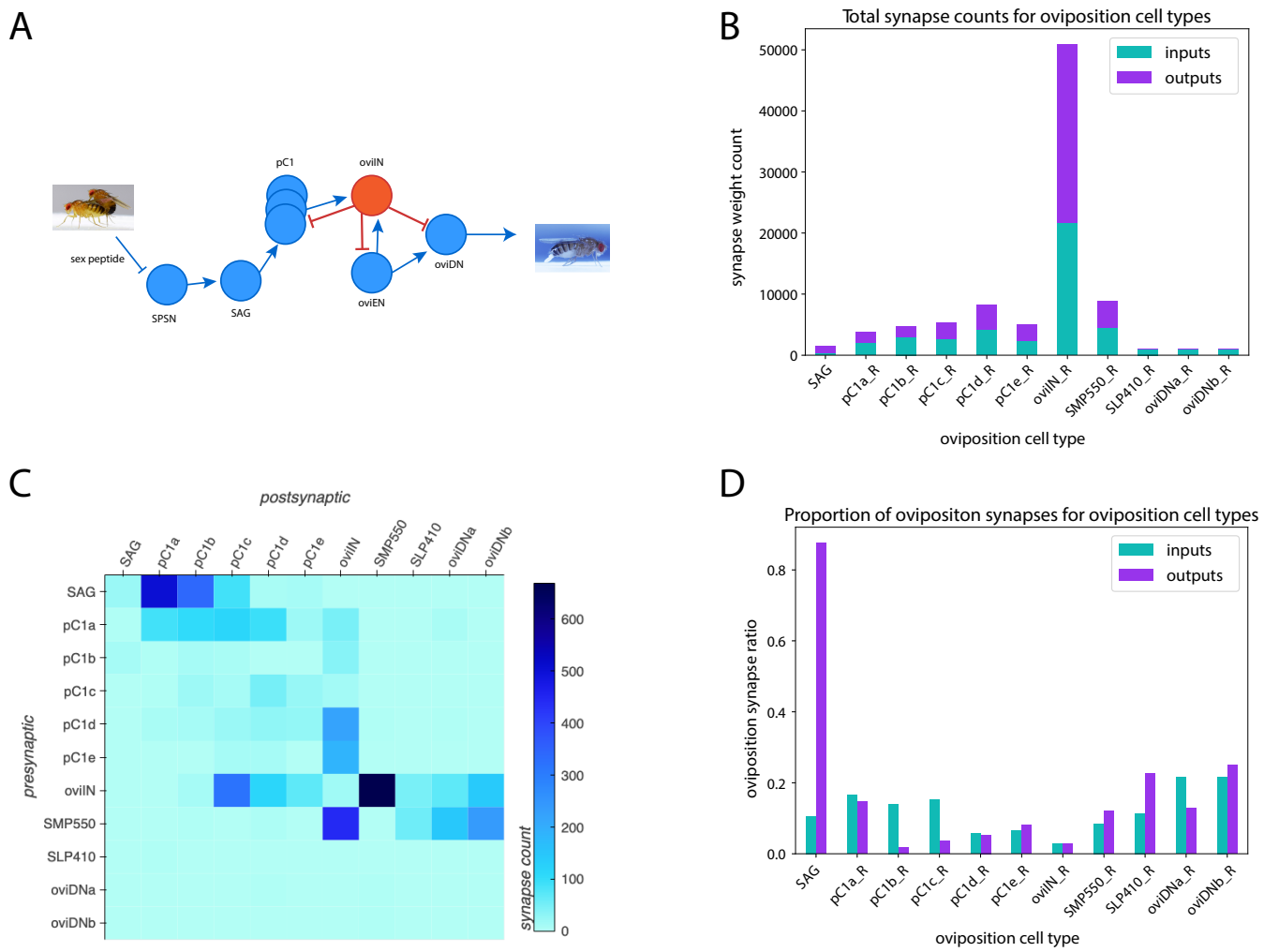

Figure 1. The connectivity profile for the oviposition circuit in the Hemibrain connectome.
A. Schematic circuit diagram of the oviposition circuit from ***Wang et al.*** (***2020***) that conveys mating status to the oviposition Descending Neurons (oviDN) which command the oviposition motor sequence. The oviIN is an inhibitory neuron in this circuit.
B. Total synapse counts for the oviposition cell types in the Hemibrain connectome. Counts are based on the number of presynaptic (inputs; teal) and postsynaptic (outputs; purple) connections. Only right instances of the oviposition cell types are included because left instances are often truncated. The mean counts are presented for the SAG and SLP410_R because they each have two instances. The SMP550 are presumed to be the oviEN, and the SLP410 are believed to be an additional pair of oviDNa (***Nojima et al., 2021***).
C. Connectivity matrix for the oviposition cell types (including right and left instances). Synapse counts are the aggregated synaptic weights from all neurons of one cell type to all neurons of another cell type.
D. The proportion of synapses that are made with other oviposition neurons. The inputs ratio (teal) for a given cell type is the proportion of synapses received from presynaptic oviposition partners relative to synapses from all presynaptic partners. The outputs ratio (purple) is the proportion of synapses to other oviposition neurons relative to synapses to all postsynaptic partners.

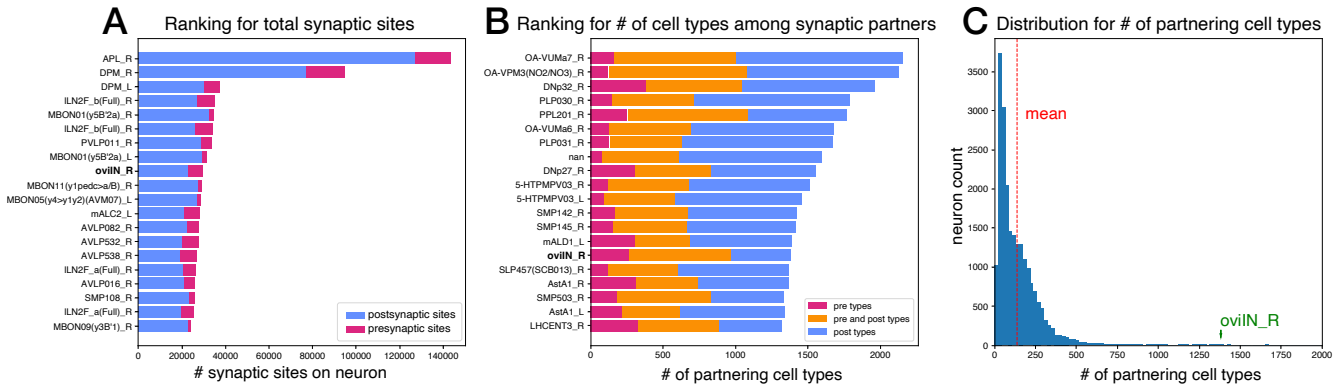

Figure 2. The oviIN is an outlier in the Hemibrain.

A. Out of the 20,000+ neurons in the Hemibrain, the top 20 neurons with the most synaptic sites (pre and post sites) on its body are ranked in descending order and labeled by their instance label from the Hemibrain. This count includes synaptic sites that are unpaired. oviIN_R ranks 9th with 29,892 synaptic sites. The APL has the most synaptic sites on its body followed by the DPM. Mean synaptic site count: 1,148.05. Mode: 2,159.71. The quantities of postsynaptic sites (blue) eclipse presynaptic sites (magenta) because Drosophila synapses are polyadic.

B. The top 20 neurons in the Hemibrain with the greatest quantity of distinct cell types among their direct synaptic partners are ranked in descending order and labeled by instance. Counts of cell types that are exclusively presynaptic are shown in magenta, exclusively postsynaptic cell types shown in blue, and counts of cell types that are both presynaptic and postsynaptic to the neuron are shown in orange. The oviIN_R ranks 15th with 1,379 total cell types (968 presynaptic and 1,112 post-synaptic cell types).

C. Histogram showing the distribution of the number of cell types among synaptic partners for all neurons in the Hemibrain. Most neurons partner with 213 cell types while oviIN_R makes direct connections with 1379 cell types.

Figure 2—figure supplement 1. The top 20 neurons in the Hemibrain with the highest total synaptic connection counts (i.e. synaptic weights). The oviIN_R ranks 6th with 50898 synaptic connections. Input weights (magenta) are counts of postsynaptic sites on the indicated neuron that are paired with a presynaptic site. Output weights (blue) are counts of postsynaptic sites that are paired with a presynaptic site that is on the indicated neuron.

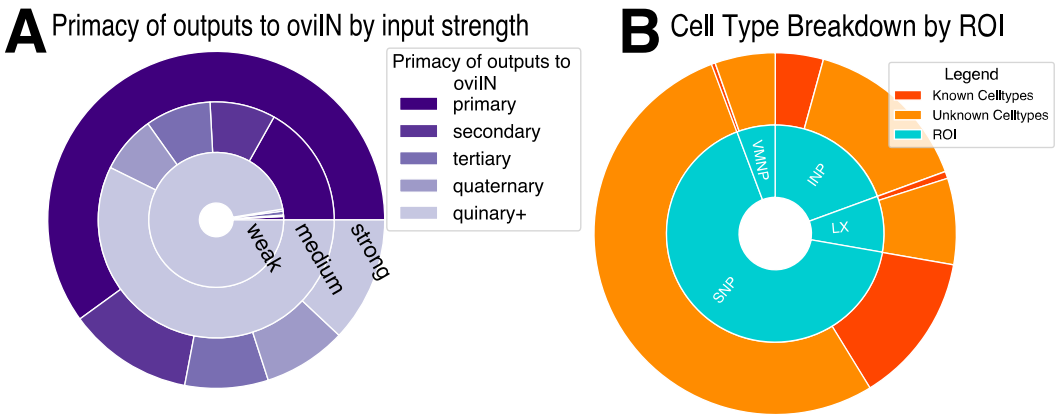

Figure 3. Characterizing the inputs to oviIN.
A. Cell types that have oviIN as their strongest output also tend to be strong inputs to oviIN. The 3 rings indicate the strength of the cell type input connections to oviIN. Synaptic input weights to oviIN were combined among neurons of the same cell type (strong: cell types with 120 or more combined connection weights; medium: less than 120 but greater than or equal to 40 combined connection weights; weak: fewer than 40 combined connection weights). The color code represents the primacy of oviIN as an output of those cell types. Primary types have oviIN as their strongest output, secondary types have oviIN as their second strongest output and so on. The wedges indicate the proportion of cell types are that primary, secondary, etc. Among the strong inputs to oviIN, the majority of cell types are primary; however, among the weak inputs to oviIN, the majority of cell types do not have oviIN as one of their top 5 outputs.
B. Inner annulus shows presynaptic connections to oviIN by the neuropil in which the connection is made. Most synapses from presynaptic neurons onto oviIN are made in the SNP. Outer annulus shows the proportions of synapses made within a neuropil where the presynaptic neuron is a known (red) or unknown type (orange). SNP contains: SMP, SIP, SLP neuropils; VMNP: AOTU, VLP, PLP, WED neuropils; INP: CRE, CL, IB, ATL neuropils; LX: BL, LAL neuropils.

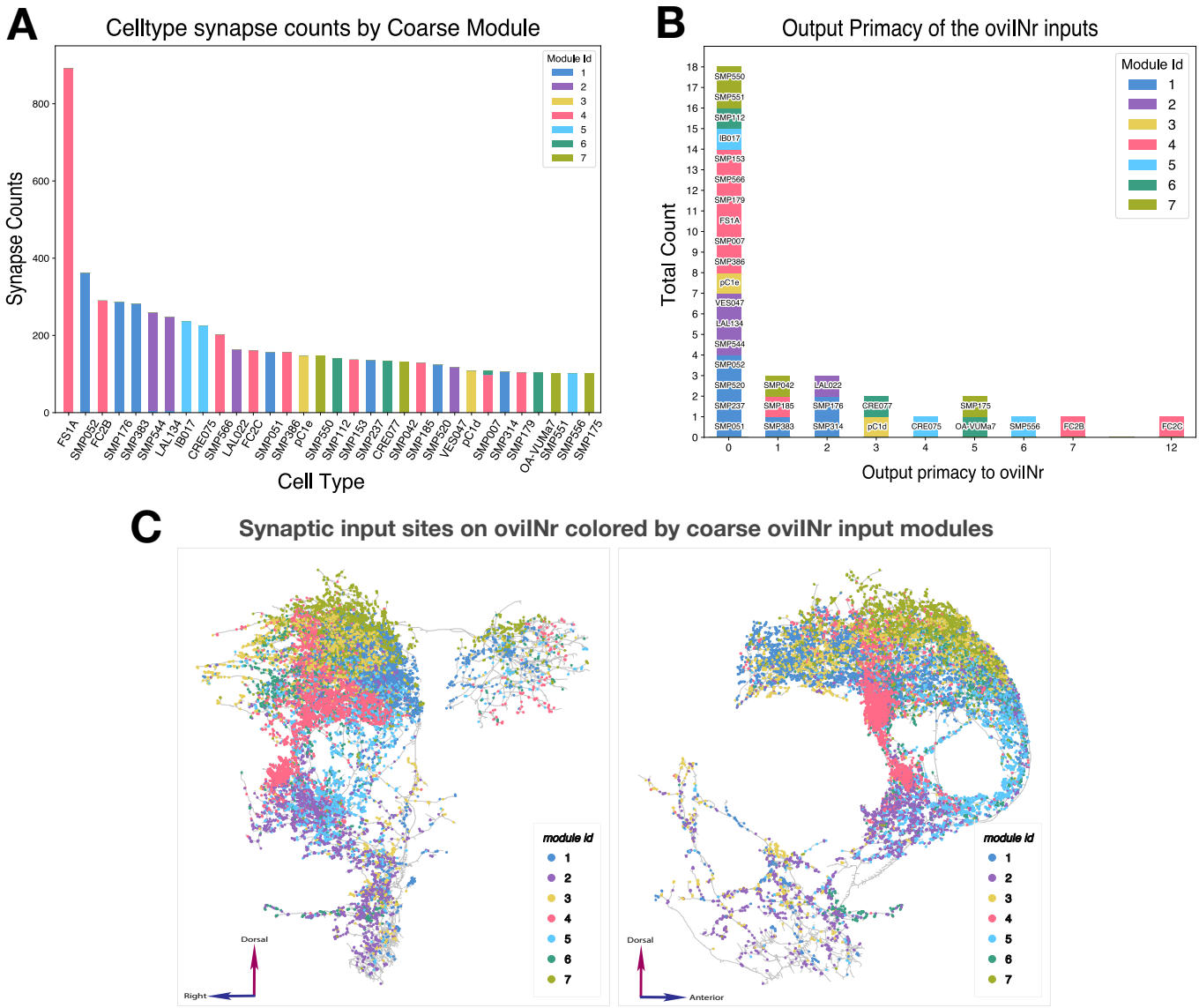

Figure 4. Modularity analysis reveals mesoscale connectome structure among inputs to oviIN.

A. Neuronal cell types that make an aggregated synapse count of at least 100 onto oviIN. The bars indicating synapse counts are color-coded by the module(s) into which the neurons of a type are grouped. Sometimes, neurons of the same type are clustered into different modules. For example, while all instances of FS1A are in module 4, three instances of SMP007 are grouped into module 4 and the other instance is grouped into module 6 (there are four instances of SMP007, all on the right side of the brain).

B. Most of the strongest inputs to oviIN are primary inputs (output primacy position = 0). The cell types with the highest aggregated connection strength (100) onto the oviIN are shown. Output primacy position was computed by oviIN's rank among the cell type's strongest outputs. Each cell type is colored according to the module where most of its instances are grouped.

C. The wire skeleton of the right oviIN from the Hemibrain is shown in gray. Each dot on the body of oviIN is a postsynaptic site. These connection sites are colored according to the module of the presynaptic neuron. Synapses from neurons without a cell type label (annotated as NaN) are not shown, but results are qualitatively the same when they are included. Left panel: front view; Right panel: lateral view from the right side of the brain.

Figure 4—figure supplement 1. Super neuropil representation in the oviIN_R's pre-synaptic partners. The counts of synapses to oviIN_R within a neuropil are used to compute the neuropil proportions. The pie chart wedges are calculated based on connection weights within an neuropil relative to the total connections in a module.

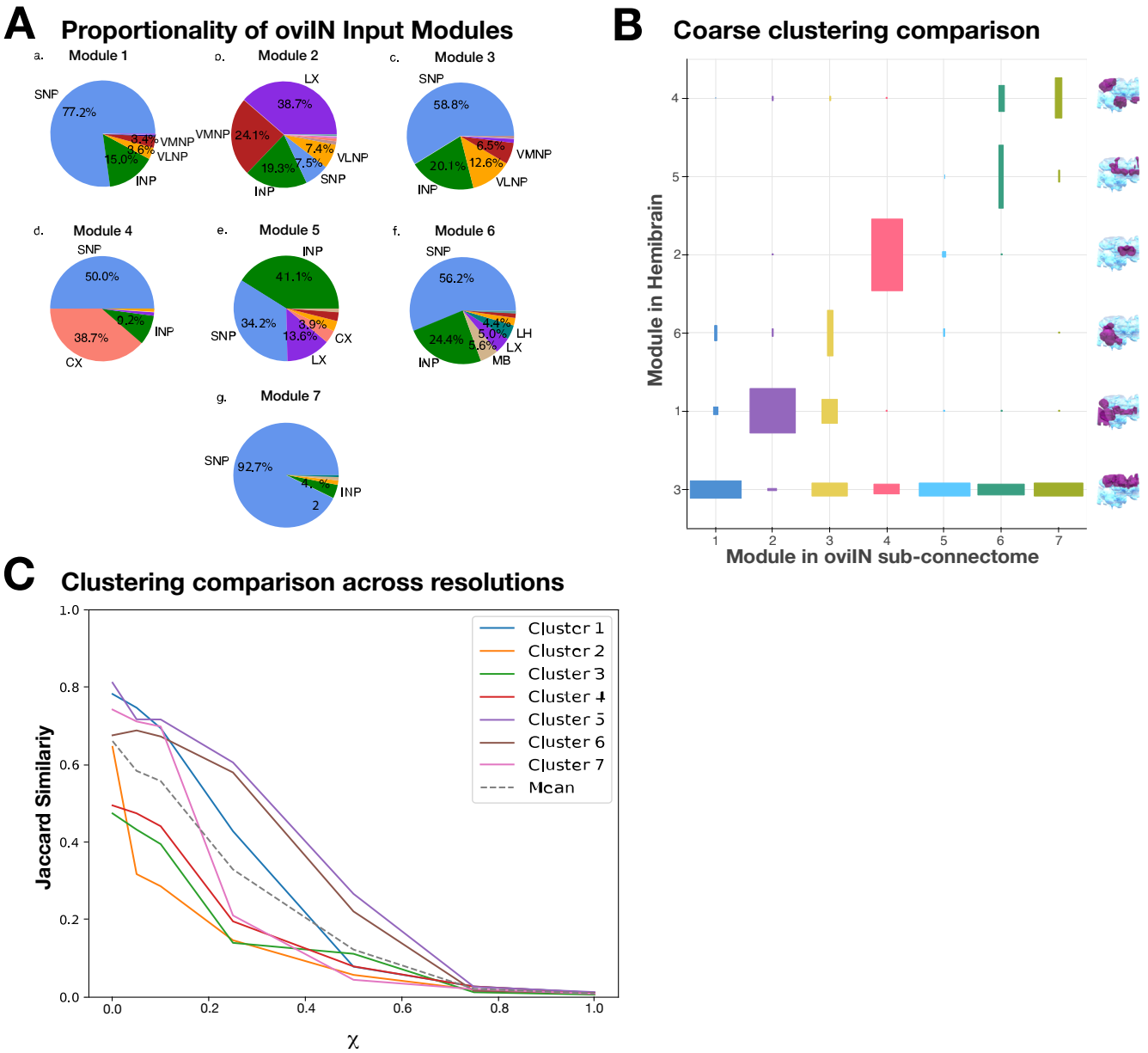

Figure 5. The modules do not align with neuropils nor whole brain modules at any resolution.
A. Proportions of super neuropils in the oviIN's sub-connectome by module. The proportions of connections made in the various super neuropils by the neurons in each module are represented as pie slices. The neurons in most of the modules make a large portion of their synapses in the SNP. The super neuropil hierarchy used is defined by ***Ito et al.*** (***2014***).
B. Modularity provides partitions of the oviIN input connectome that are distinct from partitions for the full Hemibrain connectome. Box width represents the fraction of the total neurons from a full Hemibrain module (shown on the *y* axis) contained in a module from the oviIN input connectome (shown on the *x* axis). The height is the fraction of the total number of neurons on the *x* axis corresponding to the *y* axis. Volumetric renderings of the brain regions roughly contained in each whole brain module are displayed on the right *y* axis. The colors indicate the modules of the subconnectome of oviIN's inputs.
C. Jaccard similarity between modules of the oviIN sub-connectome (solid lines) and the full connectome at various resolutions. The full connectome modules were generated using the same RenEEL algorithm as for the oviIN sub-connectome. Mean Jaccard similarity is plotted in gray (dashed line).

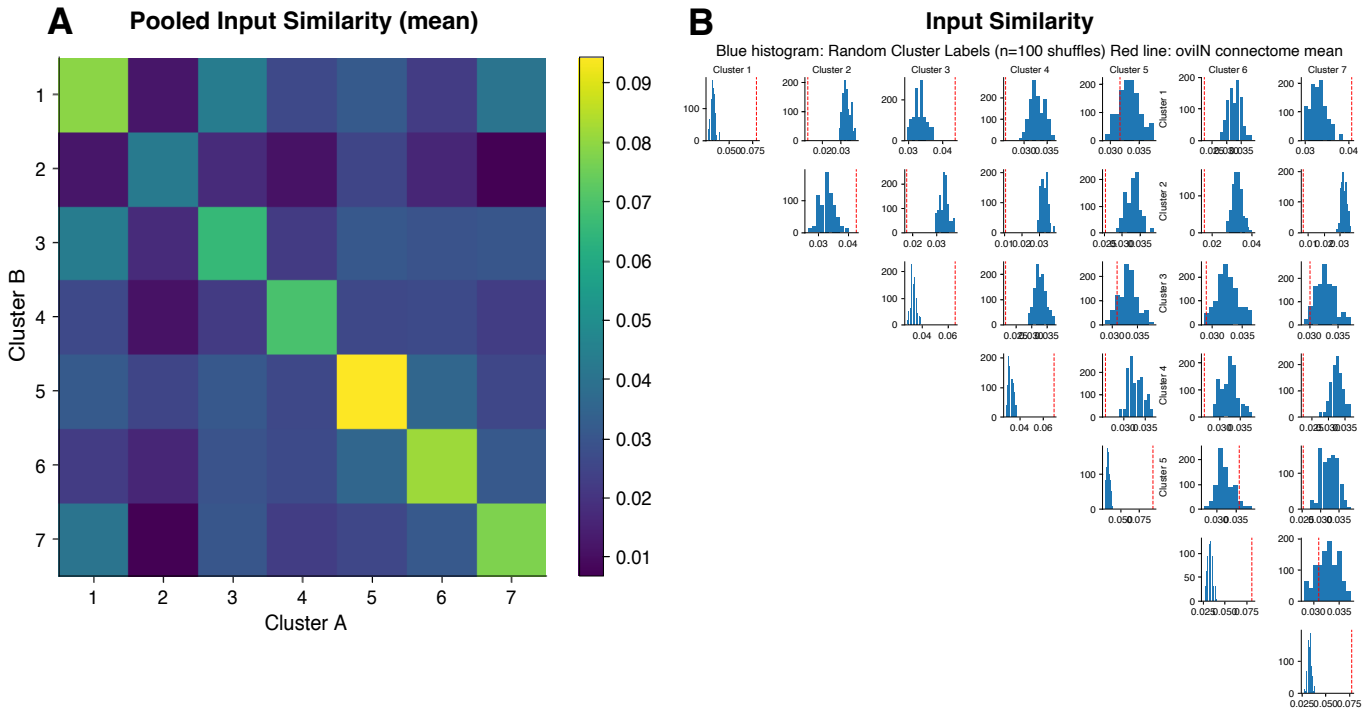

Figure 6. Module neurons have inputs in common

A. Sub-connectome neurons have higher input similarity with neurons of the same module (i.e. cluster) than with other neurons. The inputs to neurons in the sub-connectome of oviIN's inputs include direct connections from neurons anywhere in the brain. Heatmap colors indicate the mean input similarity between all neurons in cluster A vs. cluster B.

B. Randomization of module labels shows decreased similarity for all self-same cluster pairs. The input similarity is shown on the *x*-axes which ranges from 0 to 1. The counts of similarity values for pairs of neurons is shown on the *y*-axes. The red line indicates the mean input similarity between modules as visualized in *A*.

References

Aso Y, Hattori D, Yu Y, Johnston RM, Iyer NA, Ngo TT, Dionne H, Abbott L, Axel R, Tanimoto H, Rubin GM. The neuronal architecture of the mushroom body provides a logic for associative learning. eLife. 2014 Dec; 3:e04577. https://doi.org/10.7554/eLife.04577, doi: 10.7554/eLife.04577.

Aso Y, Sitaraman D, Ichinose T, Kaun KR, Vogt K, Belliart-Guérin G, Plaçais PY, Robie AA, Yamagata N, Schnaitmann C, Rowell WJ, Johnston RM, Ngo TTB, Chen N, Korff W, Nitabach MN, Heberlein U, Preat T, Branson KM, Tanimoto H, et al. Mushroom body output neurons encode valence and guide memory-based action selection in Drosophila. eLife. 2014 Dec; 3:e04580. https://doi.org/10.7554/eLife.04580, doi: 10.7554/eLife.04580.

Azanchi R, Kaun KR, Heberlein U. Competing dopamine neurons drive oviposition choice for ethanol in Drosophila. Proceedings of the National Academy of Sciences. 2013 Dec; 110(52):21153–21158. https://www.pnas.org/doi/full/10.1073/pnas.1320208110, doi: 10.1073/pnas.1320208110.

Betzel R, Puxeddu MG, Seguin C. Hierarchical communities in the larval Drosophila connectome: Links to cellular annotations and network topology. Proceedings of the National Academy of Sciences. 2024 Sep; 121(38):e2320177121. https://www.pnas.org/doi/abs/10.1073/pnas.2320177121, doi: 10.1073/pnas.2320177121, publisher: Proceedings of the National Academy of Sciences.

Chou YH, Spletter ML, Yaksi E, Leong JCS, Wilson RI, Luo L. Diversity and wiring variability of olfactory local interneurons in the Drosophila antennal lobe. Nature Neuroscience. 2010 Apr; 13(4):439–449. https://www.nature.com/articles/nn.2489, doi: 10.1038/nn.2489, publisher: Nature Publishing Group.

Chung J, Bridgeford E, Arroyo J, Pedigo BD, Saad-Eldin A, Gopalakrishnan V, Xiang L, Priebe CE, Vogelstein JT. Statistical Connectomics. Annual Review of Statistics and Its Application. 2021 Mar; 8(Volume 8, 2021):463–492. https://www.annualreviews.org/content/journals/10.1146/annurev-statistics-042720-023234, doi: 10.1146/annurev-statistics-042720-023234, publisher: Annual Reviews.

Churchill ER, Dytham C, Bridle JR, Thom MDF. Social and physical environment independently affect oviposition decisions in Drosophila. Behavioral Ecology. 2021 Nov; 32(6):1391–1399. https://doi.org/10.1093/beheco/arab105, doi: 10.1093/beheco/arab105.

Coleman RT, Morantte I, Koreman GT, Cheng ML, Ding Y, Ruta V. A modular circuit coordinates the diversification of courtship strategies. Nature. 2024 Oct; p. 1–9. https://www.nature.com/articles/s41586-024-08028-1, doi: 10.1038/s41586-024-08028-1, publisher: Nature Publishing Group.

Cury KM, Axel R. Flexible neural control of transition points within the egg-laying behavioral sequence in Drosophila. Nature Neuroscience. 2023 Jun; 26(6):1054–1067. https://www.nature.com/articles/s41593-023-01332-5, doi: 10.1038/s41593-023-01332-5, number: 6 Publisher: Nature Publishing Group.

Cury KM, Prud'homme B, Gompel N. A short guide to insect oviposition: when, where and how to lay an egg. Journal of Neurogenetics. 2019 Apr; 33(2):75–89. https://doi.org/10.1080/01677063.2019.1586898, doi: 10.1080/01677063.2019.1586898, publisher: Taylor & Francis _eprint: https://doi.org/10.1080/01677063.2019.1586898.

Deutsch D, Pacheco D, Encarnacion-Rivera L, Pereira T, Fathy R, Clemens J, Girardin C, Calhoun A, Ireland E, Burke A, Dorkenwald S, McKellar C, Macrina T, Lu R, Lee K, Kemnitz N, Ih D, Castro M, Halageri A, Jordan C, et al. The neural basis for a persistent internal state in Drosophila females. eLife. 2020 Nov; 9:e59502. https://doi.org/10.7554/eLife.59502, doi: 10.7554/eLife.59502.

Devineni AV, Sun B, Zhukovskaya A, Axel R. Acetic acid activates distinct taste pathways in Drosophila to elicit opposing, state-dependent feeding responses. eLife. 2019 Jun; 8:e47677. https://doi.org/10.7554/eLife.47677, doi: 10.7554/eLife.47677, publisher: eLife Sciences Publications, Ltd.

Dorkenwald S, Matsliah A, Sterling AR, Schlegel P, Yu Sc, McKellar CE, Lin A, Costa M, Eichler K, Yin Y, Silversmith W, Schneider-Mizell C, Jordan CS, Brittain D, Halageri A, Kuehner K, Ogedengbe O, Morey R, Gager J, Kruk K, et al. Neuronal wiring diagram of an adult brain. Nature. 2024 Oct; 634(8032):124–138. https://www.nature.com/articles/s41586-024-07558-y, doi: 10.1038/s41586-024-07558-y, publisher: Nature Publishing Group.

Feng K, Palfreyman MT, Häsemeyer M, Talsma A, Dickson BJ. Ascending SAG Neurons Control Sexual Receptivity of Drosophila Females. Neuron. 2014 Jul; 83(1):135–148. https://www.sciencedirect.com/science/article/pii/S0896627314004036, doi: 10.1016/j.neuron.2014.05.017.

Ganguly I, Heckman EL, Litwin-Kumar A, Clowney EJ, Behnia R. Diversity of visual inputs to Kenyon cells of the Drosophila mushroom body. Nature Communications. 2024 Jul; 15(1):5698. https://www.nature.com/articles/s41467-024-49616-z, doi: 10.1038/s41467-024-49616-z, publisher: Nature Publishing Group.

Griffith LC. Neuromodulatory control of sleep in Drosophila melanogaster: integration of competing and complementary behaviors. Current Opinion in Neurobiology. 2013 Oct; 23(5):819–823. https://linkinghub.elsevier.com/retrieve/pii/S0959438813001165, doi: 10.1016/j.conb.2013.05.003.

Guo J, Singh P, Bassler KE. Reduced network extremal ensemble learning (RenEEL) scheme for community detection in complex networks. Scientific Reports. 2019 Oct; 9(1):14234. https://www.nature.com/articles/s41598-019-50739-3, doi: 10.1038/s41598-019-50739-3, number: 1 Publisher: Nature Publishing Group.

Guo J, Singh P, Bassler KE. Resolution limit revisited: community detection using generalized modularity density. Journal of Physics: Complexity. 2023 Mar; 4(2):025001. https://dx.doi.org/10.1088/2632-072X/acc4a4, doi: 10.1088/2632-072X/acc4a4, publisher: IOP Publishing.

Haberkern H, Jayaraman V. Studying small brains to understand the building blocks of cognition. Current Opinion in Neurobiology. 2016 Apr; 37:59–65. https://www.sciencedirect.com/science/article/pii/S0959438816000088, doi: 10.1016/j.conb.2016.01.007.

Handler A, Graham TGW, Cohn R, Morantte I, Siliciano AF, Zeng J, Li Y, Ruta V. Distinct Dopamine Receptor Pathways Underlie the Temporal Sensitivity of Associative Learning. Cell. 2019 Jun; 178(1):60–75.e19. https://www.sciencedirect.com/science/article/pii/S0092867419306117, doi: 10.1016/j.cell.2019.05.040.

Haynes PR, Christmann BL, Griffith LC. A single pair of neurons links sleep to memory consolidation in Drosophila melanogaster. eLife. 2015 Jan; 4:e03868. https://doi.org/10.7554/eLife.03868, doi: 10.7554/eLife.03868.

Hindmarsh Sten T, Li R, Otopalik A, Ruta V. Sexual arousal gates visual processing during Drosophila courtship. Nature. 2021 Jul; 595(7868):549–553. https://www.nature.com/articles/s41586-021-03714-w, doi: 10.1038/s41586-021-03714-w, publisher: Nature Publishing Group.

Hulse BK, Haberkern H, Franconville R, Turner-Evans DB, Takemura Sy, Wolff T, Noorman M, Dreher M, Dan C, Parekh R, Hermundstad AM, Rubin GM, Jayaraman V. A connectome of the Drosophila central complex reveals network motifs suitable for flexible navigation and context-dependent action selection. eLife. 2021 Oct; 10:e66039. https://elifesciences.org/articles/66039, doi: 10.7554/eLife.66039.

Ito K, Shinomiya K, Ito M, Armstrong JD, Boyan G, Hartenstein V, Harzsch S, Heisenberg M, Homberg U, Jenett A, Keshishian H, Restifo LL, Rössler W, Simpson JH, Strausfeld NJ, Strauss R, Vosshall LB. A Systematic Nomenclature for the Insect Brain. Neuron. 2014 Feb; 81(4):755–765. https://www.sciencedirect.com/science/article/pii/S0896627313011781, doi: 10.1016/j.neuron.2013.12.017.

Jacobs RV, Wang CX, Nguyen L, Pruitt TJ, Wang P, Lozada-Perdomo FV, Deere JU, Liphart HA, Devineni AV. Overlap and divergence of neural circuits mediating distinct behavioral responses to sugar. Cell Reports. 2024 Oct; 43(10):114782. https://www.sciencedirect.com/science/article/pii/S2211124724011331, doi: 10.1016/j.celrep.2024.114782.

Jeanne JM, Fişek M, Wilson RI. The Organization of Projections from Olfactory Glomeruli onto Higher-Order Neurons. Neuron. 2018 Jun; 98(6):1198–1213.e6. https://www.cell.com/neuron/abstract/S0896-6273(18)30383-0, doi: 10.1016/j.neuron.2018.05.011.

Joseph RM, Devineni AV, King IFG, Heberlein U. Oviposition preference for and positional avoidance of acetic acid provide a model for competing behavioral drives in Drosophila. Proceedings of the National Academy of Sciences. 2009 Jul; 106(27):11352–11357. https://www.pnas.org/doi/full/10.1073/pnas.0901419106, doi: 10.1073/pnas.0901419106.

Jourjine N, Mullaney BC, Mann K, Scott K. Coupled Sensing of Hunger and Thirst Signals Balances Sugar and Water Consumption. Cell. 2016 Aug; 166(4):855–866. https://www.sciencedirect.com/science/article/pii/S0092867416308546, doi: 10.1016/j.cell.2016.06.046.

Keene AC, Krashes MJ, Leung B, Bernard JA, Waddell S. *Drosophila* Dorsal Paired Medial Neurons Provide a General Mechanism for Memory Consolidation. Current Biology. 2006 Aug; 16(15):1524–1530. https://www.sciencedirect.com/science/article/pii/S0960982206017076, doi: 10.1016/j.cub.2006.06.022.

Keene AC, Stratmann M, Keller A, Perrat PN, Vosshall LB, Waddell S. Diverse Odor-Conditioned Memories Require Uniquely Timed Dorsal Paired Medial Neuron Output. Neuron. 2004 Oct; 44(3):521–533. https://www.sciencedirect.com/science/article/pii/S0896627304006476, doi: 10.1016/j.neuron.2004.10.006.

Kim H, Kirkhart C, Scott K. Long-range projection neurons in the taste circuit of Drosophila. eLife. 2017 Feb; 6:e23386. https://doi.org/10.7554/eLife.23386, doi: 10.7554/eLife.23386.

Kunin AB, Guo J, Bassler KE, Pitkow X, Josić K. Hierarchical Modular Structure of the Drosophila Connectome. Journal of Neuroscience. 2023 Sep; 43(37):6384–6400. https://www.jneurosci.org/content/43/37/6384, doi: 10.1523/JNEUROSCI.0134-23.2023, publisher: Society for Neuroscience Section: Research Articles.

Landayan D, Wang BP, Zhou J, Wolf FW. Thirst interneurons that promote water seeking and limit feeding behavior in Drosophila. eLife. 2021 May; 10:e66286. https://www.ncbi.nlm.nih.gov/pmc/articles/PMC8139827/, doi: 10.7554/eLife.66286.

Laturney M, Sterne GR, Scott K. Mating activates neuroendocrine pathways signaling hunger in Drosophila females. eLife. 2023 May; 12:e85117. https://doi.org/10.7554/eLife.85117, doi: 10.7554/eLife.85117.

Li F, Lindsey JW, Marin EC, Otto N, Dreher M, Dempsey G, Stark I, Bates AS, Pleijzier MW, Schlegel P, Nern A, Takemura Sy, Eckstein N, Yang T, Francis A, Braun A, Parekh R, Costa M, Scheffer LK, Aso Y, et al. The connectome of the adult Drosophila mushroom body provides insights into function. eLife. 2020 Dec; 9:e62576. https://doi.org/10.7554/eLife.62576, doi: 10.7554/eLife.62576.

Li MT, Cao LH, Xiao N, Tang M, Deng B, Yang T, Yoshii T, Luo DG. Hub-organized parallel circuits of central circadian pacemaker neurons for visual photoentrainment in Drosophila. Nature Communications. 2018 Oct; 9(1):4247. https://www.nature.com/articles/s41467-018-06506-5, doi: 10.1038/s41467-018-06506-5, publisher: Nature Publishing Group.

Lin A, Yang R, Dorkenwald S, Matsliah A, Sterling AR, Schlegel P, Yu Sc, McKellar CE, Costa M, Eichler K, Bates AS, Eckstein N, Funke J, Jefferis GSXE, Murthy M. Network statistics of the whole-brain connectome of Drosophila. Nature. 2024 Oct; 634(8032):153–165. https://www.nature.com/articles/s41586-024-07968-y, doi: 10.1038/s41586-024-07968-y, publisher: Nature Publishing Group.

Marquis M, Wilson RI. Locomotor and olfactory responses in dopamine neurons of the Drosophila superior-lateral brain. Current Biology. 2022 Dec; 32(24):5406–5414.e5. https://www.sciencedirect.com/science/article/pii/S096098222201764X, doi: 10.1016/j.cub.2022.11.008.

Matsliah A, Yu Sc, Kruk K, Bland D, Burke AT, Gager J, Hebditch J, Silverman B, Willie KP, Willie R, Sorek M, Sterling AR, Kind E, Garner D, Sancer G, Wernet MF, Kim SS, Murthy M, Seung HS. Neuronal parts list and wiring diagram for a visual system. Nature. 2024 Oct; 634(8032):166–180. https://www.nature.com/articles/s41586-024-07981-1, doi: 10.1038/s41586-024-07981-1, publisher: Nature Publishing Group.

Newman MEJ. Modularity and community structure in networks. Proceedings of the National Academy of Sciences. 2006 Jun; 103(23):8577–8582. https://www.pnas.org/doi/full/10.1073/pnas.0601602103, doi: 10.1073/pnas.0601602103, publisher: Proceedings of the National Academy of Sciences.

Newman MEJ, Girvan M. Finding and evaluating community structure in networks. Physical Review E. 2004 Feb; 69(2):026113. https://link.aps.org/doi/10.1103/PhysRevE.69.026113, doi: 10.1103/PhysRevE.69.026113, publisher: American Physical Society.

Nojima T, Rings A, Allen AM, Otto N, Verschut TA, Billeter JC, Neville MC, Goodwin SF. A sex-specific switch between visual and olfactory inputs underlies adaptive sex differences in behavior. Current Biology. 2021 Mar; 31(6):1175–1191.e6. https://www.cell.com/current-biology/abstract/S0960-9822(20)31899-6, doi: 10.1016/j.cub.2020.12.047, publisher: Elsevier.

O'Leary T, Marder E. Mapping Neural Activation onto Behavior in an Entire Animal. Science. 2014 Apr; 344(6182):372–373. https://www.science.org/doi/10.1126/science.1253853, doi: 10.1126/science.1253853.

Oram TB, Card GM. Context-dependent control of behavior in Drosophila. Current Opinion in Neurobiology. 2022 Apr; 73:102523. https://www.sciencedirect.com/science/article/pii/S0959438822000083, doi: 10.1016/j.conb.2022.02.003.

Pitman JL, Huetteroth W, Burke CJ, Krashes MJ, Lai SL, Lee T, Waddell S. A Pair of Inhibitory Neurons Are Required to Sustain Labile Memory in the *Drosophila* Mushroom Body. Current Biology. 2011 May; 21(10):855–861. https://www.sciencedirect.com/science/article/pii/S0960982211003903, doi: 10.1016/j.cub.2011.03.069.

Prisco L, Deimel SH, Yeliseyeva H, Fiala A, Tavosanis G. The anterior paired lateral neuron normalizes odour-evoked activity in the Drosophila mushroom body calyx. eLife. 2021 Dec; 10:e74172. https://doi.org/10.7554/eLife.74172, doi: 10.7554/eLife.74172, publisher: eLife Sciences Publications, Ltd.

Rockwell RF, Grossfield J. Drosophila: Behavioral Cues for Oviposition. The American Midland Naturalist. 1978; 99(2):361–368. https://www.jstor.org/stable/2424813, doi: 10.2307/2424813.

Roemschied FA, Pacheco DA, Aragon MJ, Ireland EC, Li X, Thieringer K, Pang R, Murthy M. Flexible circuit mechanisms for context-dependent song sequencing. Nature. 2023 Oct; 622(7984):794–801. https://www.nature.com/articles/s41586-023-06632-1, doi: 10.1038/s41586-023-06632-1, publisher: Nature Publishing Group.

Ruta V, Datta SR, Vasconcelos ML, Freeland J, Looger LL, Axel R. A dimorphic pheromone circuit in Drosophila from sensory input to descending output. Nature. 2010 Dec; 468(7324):686–690. https://www.nature.com/articles/nature09554, doi: 10.1038/nature09554, publisher: Nature Publishing Group.

Sayin S, De Backer JF, Siju KP, Wosniack ME, Lewis LP, Frisch LM, Gansen B, Schlegel P, Edmondson-Stait A, Sharifi N, Fisher CB, Calle-Schuler SA, Lauritzen JS, Bock DD, Costa M, Jefferis GSXE, Gjorgjieva J, Grunwald Kadow IC. A Neural Circuit Arbitrates between Persistence and Withdrawal in Hungry *Drosophila*. Neuron. 2019 Nov; 104(3):544–558.e6. https://www.sciencedirect.com/science/article/pii/S0896627319306543, doi: 10.1016/j.neuron.2019.07.028.

Scheffer LK, Meinertzhagen IA. A connectome is not enough – what is still needed to understand the brain of Drosophila? Journal of Experimental Biology. 2021 Oct; 224(21):jeb242740. https://doi.org/10.1242/jeb.242740, doi: 10.1242/jeb.242740.

Scheffer LK, Xu CS, Januszewski M, Lu Z, Takemura Sy, Hayworth KJ, Huang GB, Shinomiya K, Maitlin-Shepard J, Berg S, Clements J, Hubbard PM, Katz WT, Umayam L, Zhao T, Ackerman D, Blakely T, Bogovic J, Dolafi T, Kainmueller D, et al. A connectome and analysis of the adult Drosophila central brain. eLife. 2020 Sep; 9:e57443. https://elifesciences.org/articles/57443, doi: 10.7554/eLife.57443.

Schlegel P, Yin Y, Bates AS, Dorkenwald S, Eichler K, Brooks P, Han DS, Gkantia M, dos Santos M, Munnelly EJ, Badalamente G, Serratosa Capdevila L, Sane VA, Fragniere AMC, Kiassat L, Pleijzier MW, Stürner T, Tamimi IFM, Dunne CR, Salgarella I, et al. Whole-brain annotation and multi-connectome cell typing of Drosophila. Nature. 2024 Oct; 634(8032):139–152. https://www.nature.com/articles/s41586-024-07686-5, doi: 10.1038/s41586-024-07686-5, publisher: Nature Publishing Group.

Schwartz NU, Zhong L, Bellemer A, Tracey WD. Egg Laying Decisions in Drosophila Are Consistent with Foraging Costs of Larval Progeny. PLOS ONE. 2012 May; 7(5):e37910. https://journals.plos.org/plosone/article?id=10.1371/journal.pone.0037910, doi: 10.1371/journal.pone.0037910.

Shafer OT, Gutierrez GJ, Li K, Mildenhall A, Spira D, Marty J, Lazar AA, Fernandez MdlP. Connectomic analysis of the Drosophila lateral neuron clock cells reveals the synaptic basis of functional pacemaker classes. eLife. 2022 Jun; 11:e79139. https://doi.org/10.7554/eLife.79139, doi: 10.7554/eLife.79139, publisher: eLife Sciences Publications, Ltd.

Shelly TE. Defense of Oviposition Sites by Female Oriental Fruit Flies (Diptera: Tephritidae). The Florida Entomologist. 1999; 82(2):339–346. https://www.jstor.org/stable/3496587, doi: 10.2307/3496587.

Taisz I, Donà E, Münch D, Bailey SN, Morris BJ, Meechan KI, Stevens KM, Varela-Martínez I, Gkantia M, Schlegel P, Ribeiro C, Jefferis GSXE, Galili DS. Generating parallel representations of position and identity in the olfactory system. Cell. 2023 Jun; 186(12):2556–2573.e22. https://www.sciencedirect.com/science/article/pii/S0092867423004725, doi: 10.1016/j.cell.2023.04.038.

Vijayan V, Wang F, Wang K, Chakravorty A, Adachi A, Akhlaghpour H, Dickson BJ, Maimon G. A rise-to-threshold process for a relative-value decision. Nature. 2023 Jul; 619(7970):563–571. https://www.nature.com/articles/s41586-023-06271-6, doi: 10.1038/s41586-023-06271-6, number: 7970 Publisher: Nature Publishing Group.

Vijayan V, Wang Z, Chandra V, Chakravorty A, Li R, Sarbanes SL, Akhlaghpour H, Maimon G. An internal expectation guides Drosophila egg-laying decisions. Science Advances. 2022 Oct; 8(43):eabn3852. https://www.ncbi.nlm.nih.gov/pmc/articles/PMC9616500/, doi: 10.1126/sciadv.abn3852.

Waddell S, Armstrong JD, Kitamoto T, Kaiser K, Quinn WG. The *amnesiac* Gene Product Is Expressed in Two Neurons in the *Drosophila* Brain that Are Critical for Memory. Cell. 2000 Nov; 103(5):805–813. https://www.sciencedirect.com/science/article/pii/S0092867400001835, doi: 10.1016/S0092-8674(00)00183-5.

Walker SR, Peña-Garcia M, Devineni AV. Connectomic analysis of taste circuits in Drosophila. bioRxiv: The Preprint Server for Biology. 2024 Sep; p. 2024.09.14.613080. doi: 10.1101/2024.09.14.613080.

Wang F, Wang K, Forknall N, Patrick C, Yang T, Parekh R, Bock D, Dickson BJ. Neural circuitry linking mating and egg laying in Drosophila females. Nature. 2020 Mar; 579(7797):101–105. http://www.nature.com/articles/s41586-020-2055-9, doi: 10.1038/s41586-020-2055-9.

Wang K, Gong J, Wang Q, Li H, Cheng Q, Liu Y, Zeng S, Wang Z. Parallel pathways convey olfactory information with opposite polarities in Drosophila. Proceedings of the National Academy of Sciences. 2014 Feb; 111(8):3164–3169. https://www.pnas.org/doi/full/10.1073/pnas.1317911111, doi: 10.1073/pnas.1317911111, publisher: Proceedings of the National Academy of Sciences.

Winding M, Pedigo BD, Barnes CL, Patsolic HG, Park Y, Kazimiers T, Fushiki A, Andrade IV, Khandelwal A, Valdes-Aleman J, Li F, Randel N, Barsotti E, Correia A, Fetter RD, Hartenstein V, Priebe CE, Vogelstein JT, Cardona A, Zlatic M. The connectome of an insect brain. Science. 2023 Mar; 379(6636):eadd9330. https://www.science.org/doi/10.1126/science.add9330, doi: 10.1126/science.add9330, publisher: American Association for the Advancement of Science.

Yang Ch, Belawat P, Hafen E, Jan LY, Jan YN. Drosophila Egg-Laying Site Selection as a System to Study Simple Decision-Making Processes. Science. 2008 Mar; 319(5870):1679–1683. https://www.science.org/doi/10.1126/science.1151842, doi: 10.1126/science.1151842, publisher: American Association for the Advancement of Science.

Yang CH, He R, Stern U. Behavioral and Circuit Basis of Sucrose Rejection by Drosophila Females in a Simple Decision-Making Task. Journal of Neuroscience. 2015 Jan; 35(4):1396–1410. https://www.jneurosci.org/content/35/4/1396, doi: 10.1523/JNEUROSCI.0992-14.2015.

Yang Ch, Rumpf S, Xiang Y, Gordon MD, Song W, Jan LY, Jan YN. Control of the Postmating Behavioral Switch in Drosophila Females by Internal Sensory Neurons. Neuron. 2009 Feb; 61(4):519–526. https://www.sciencedirect.com/science/article/pii/S0896627308010933, doi: 10.1016/j.neuron.2008.12.021.

Zhang L, Yu J, Guo X, Wei J, Liu T, Zhang W. Parallel Mechanosensory Pathways Direct Oviposition Decision-Making in *Drosophila*. Current Biology. 2020 Aug; 30(16):3075–3088.e4. https://www.sciencedirect.com/science/article/pii/S0960982220307636, doi: 10.1016/j.cub.2020.05.076.

Zhou C, Pan Y, Robinett CC, Meissner GW, Baker BS. Central Brain Neurons Expressing *doublesex* Regulate Female Receptivity in *Drosophila*. Neuron. 2014 Jul; 83(1):149–163. https://www.sciencedirect.com/science/article/pii/S0896627314004826, doi: 10.1016/j.neuron.2014.05.038.

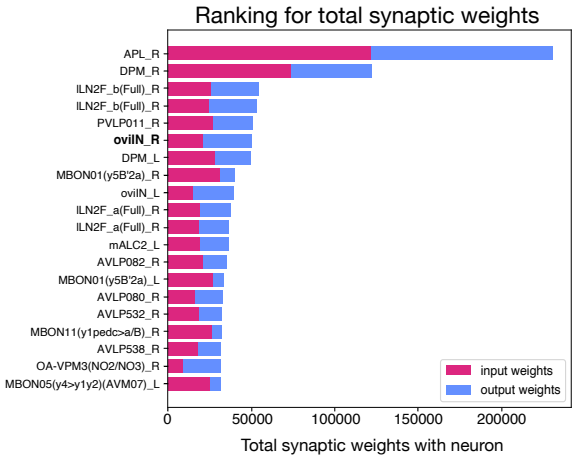

Figure 2—figure supplement 1. The top 20 neurons in the Hemibrain with the highest total synaptic connection counts (i.e. synaptic weights). The oviIN_R ranks 6th with 50898 synaptic connections. Input weights (magenta) are counts of postsynaptic sites on the indicated neuron that are paired with a presynaptic site. Output weights (blue) are counts of postsynaptic sites that are paired with a presynaptic site that is on the indicated neuron.

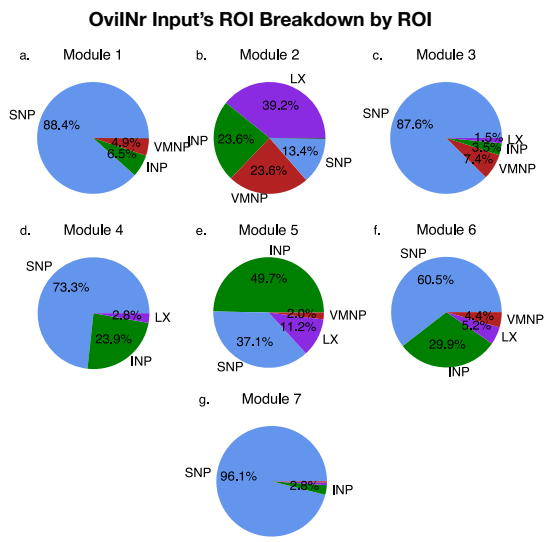

Figure 4—figure supplement 1. Super neuropil representation in the oviIN_R's pre-synaptic partners. The counts of synapses to oviIN_R within a neuropil are used to compute the neuropil proportions. The pie chart wedges are calculated based on connection weights within an neuropil relative to the total connections in a module.